Section V.B Production of UCN in superfluid ^{4}He

Recent neutron EDM experiments were limited by the UCN flux produced in cold moderators. The Liouville theorem dictates that the phase space density of UCN can not be increased beyond its value in the source moderator by, for example, gravitational deceleration or reflection from a moving surface. In 1975, Golub and Pendlebury [1] pointed out that UCNs produced via an inelastic down-scattering process in certain moderator materials could achieve much higher UCN densities than in conventional moderators. In particular, they suggested [2] that superfluid ^4He has many unique features making it an ideal moderator for producing an intense source of UCN. In this so-called "superthermal" UCN source, the incident neutrons do not reach thermal equilibrium with the moderator.

The underlying principle of a superthermal UCN source can be appreciated [3] by considering a moderator with only two energy levels: a ground state and an excited state of excitation energy Δ. An incident neutron with energy near Δ could excite the inelastic level of the moderator and lose almost all its energy to become an UCN (the "down-scattering process"). However, the UCN could later regain some energy by interacting with the excited states of the moderator and cease to be an UCN (the "up-scattering" process). To maintain a high density of UCN, it is necessary to minimize the up-scattering probability. The principle of detailed balance demands that the up-scattering cross section, σ_{UP}, is related to the down-scattering cross section, σ_{DOWN}, by the expression

$$E_{UCN}\ \sigma_{UP} = (E_{UCN} + \Delta)\ e^{-\Delta/kT}\ \sigma_{DOWN}, \tag{1}$$

where k is the Boltzmann constant and T is the temperature of the moderator. Typically, σ_{DOWN} is practically independent of T and Eq. 1 shows that the up-scattering cross section can be made arbitrarily small by lowering the temperature until $kT << \Delta$. Therefore, the UCN density could reach a value $\sim (E_{UCN}/\Delta)e^{\Delta/kT}$ in such a superthermal source. This is to be contrasted with conventional moderators in which the UCN density is proportional to $1/T^2$.

In rare situations, the materials suitable for producing UCN via the superthermal process are also ideal for storing the UCN. Superfluid ^4He is such a material. The tightly bound ^4He nucleus allows no neutron absorption, and no UCN can be lost due to absorption on ^4He. As mentioned above, the UCN can still be lost via the up-scattering process, which fortunately can be minimized by decreasing the superfluid ^4He temperature.

Several experiments have been performed to study the production and storage of UCN in superfluid ^4He [4, 5, 6, 7, 8, 9]. Evidence for UCN production has been reported in these experiments, although the observed UCN production rate was not always in agreement with the theoretical expectation [7, 10, 11]. A most recent neutron lifetime experiment carried out at NIST [8, 9] made use of this technique for UCN production, and the observed production rate was found to be consistent with the theoretical expectation.

In the following sections, we summarize the charateristics of the interaction of cold neutron beam with superfluid ^4He. Results of numerical calculations for the UCN production rate using the proposed cold neutron source and the proposed beam line at LANSCE will also be presented.

V.B.1 UCN production via the single – phonon process

The study of the interaction of cold neutron with condensed matter has a long history. Placzek and Van Hove first pointed out that the energy-versus-momentum relation, i.e. the dispersion curve, of a solid could be measured with cold neutrons inelastically scattered from the solid [12]. Cohen and Feynman [13] suggested that the dispersion curve in liquid helium could also be directly determined via this technique. Consider a neutron of incident momentum $\hbar\mathbf{k_i}$ inelastically scattered from superfluid ^4He to a momentum of $\hbar\mathbf{k_f}$ while the superfluid is excited into a state of excitation energy E. Conservation of energy and momentum requires

$$\mathbf{Q} = \mathbf{k_i} - \mathbf{k_f}, \tag{2}$$

and

$$\hbar^2 k_i^2/2m = \hbar^2 k_f^2/2m + E(Q), \tag{3}$$

where $\hbar\mathbf{Q}$ is the momentum transfer and $E(Q)$ is the energy-versus-momentum dispersion relation for superfluid ^4He. For single-phonon excitation, the Landau-Feynman dispersion curve has been well determined from neutron scattering experiments. In Fig. 1 the data from a measurement of Cowley and Woods [14] are shown. For the low momentum region ($Q < 1\mathring{A}^{-1}$), the dispersion relation is approximately linear and is well parameterized [15] as

$$\omega = aQ(1 + \gamma Q^2 \frac{1 - Q^2/Q_A^2}{1 + Q^2/Q_B^2}), \tag{4}$$

where $a = 2.383 \times 10^4$ cm/sec, $\gamma = 1.112\mathring{A}^2$, $Q_A = 0.5418\mathring{A}^{-1}$, and $Q_B = 0.3322\mathring{A}^{-1}$. This parameterization is shown as the dotted curve in Fig. 1.

At certain beam momenta, the incident neutron can transfer practically all its momentum (and energy) to the phonon and emerge as an UCN. This condition is met when the free-neutron dispersion curve intersects the dispersion curve of the superfluid ^4He. Using the above parameterization for the single-phonon excitation, this occurs at $k_i = 0.7038\mathring{A}^{-1}$ (or $\lambda \equiv 2\pi/k = 8.928\mathring{A}$), as shown in Fig. 1. We call this momentum the "critical momentum" k_c. For a neutron beam with momentum near k_c, a phonon emitted along the beam direction would carry off essentially all the beam energy and leave an UCN behind.

It is clear that UCN can be produced only for neutrons scattered into certain angles. To illustrate this point, Eqs. 2 and 3 can be solved numerically for k_f as a function of k_i and θ, the neutron laboratory scattering angle. In Fig. 2 we show results of the calculation for several incident neutron momenta. Several remarks are in order:

1. At $\theta = 0°$, there is always a solution, $k_f = k_i$, corresponding to an elastic scattering.

2. For $k_i > k_c$, all scattering angles are allowed for the neutrons.

3. For $k_i < k_c$, only $\theta < 90°$ is allowed. For each allowed scattering angle, there exist two solutions for k_f.

4. For $k_i < 0.3777\mathring{A}^{-1}$, no inelastic scattering is allowed, and the neutron beam will traverse the superfluid ^4He without attenuation. At $k = 0.3777\mathring{A}^{-1}$, the group velocities, $d\omega/dk$, for free neutrons and phonons are identical. Below this momentum, phonons travel faster than neutrons.

The horizontal dashed curve in Fig. 2 corresponds to 200 nev, a typical wall potential for UCN bottles. For neutrons emerging with k_f below the dashed curve, they can be stored as UCNs. Figure 2 shows that only neutrons with k_i very close to k_c are capable of generating UCNs. It is worth noting that for $k_i > k_c$, UCNs are predominantly produced at $\theta > 90°$. In contrast, UCNs are only produced at $\theta < 90°$ for $k_i < k_c$.

To evaluate the UCN production cross sections, we use the following expression from Cohen and Feynman [13] (See Ref. [10] for a detailed derivation):

$$\frac{d\sigma}{d\Omega} = a^2 \frac{k_f}{k_i} \frac{Z(Q)}{|1 + \frac{M_n}{\hbar^2}\frac{E'(Q)}{Q}(1 - \frac{k_i}{k_f}cos\theta)|}, \tag{5}$$

where a is the scattering length of neutron on a bound ^4He nucleus ($4\pi a^2 = 1.1 \pm 0.15$ barns [16]), M_n is the neutron mass, $E'(Q)$ is the derivative of the ^4He dispersion curve, and $Z(Q)$ is the single-phonon structure factor for ^4He. From the strength of the single-phonon peak measured in neutron scattering experiments, $Z(Q)$ is well determined experimentally. Figure 3(a) shows the data for the low momentum region ($Q < 1\mathring{A}^{-1}$), while Fig. 3(b) shows the $Z(Q)$ data over a broader range covering roton excitations [14]. The solid curve in Fig. 3(a) corresponds to the following parameterization [14]:

$$Z(Q) = \frac{\hbar Q}{2Ms}(1 - 1.5\ Q^2 + 0.9\ Q^4), \tag{6}$$

where s is the sound velocity in ^4He ($s = 238.3\ cm/sec$), M is the mass of ^4He, and Q is in unit of $\mathring{A}^{-1}$. Note that $Z(Q)$ exhibits a peak near the roton minimum (near $Q = 2.0\mathring{A}^{-1}$). The solid curve in Fig. 3(b) is a parameterization of $Z(Q)$:

$$Z(Q) = \frac{\hbar Q}{2Ms}(1 - 1.5\ Q^2 + 0.9\ Q^4) \qquad \text{for } 0 \le Q \le 0.918\mathring{A}^{-1}; \tag{7}$$

$$Z(Q) = 0.688\ Q^2 - 1.285\ Q + 0.715 \qquad \text{for } 0.918 \le Q \le 1.787\mathring{A}^{-1}; \tag{8}$$

$$Z(Q) = 0.93 - 5.8(Q - 2.02)^2 \qquad \text{for } 1.787 \le Q \le 2.35\mathring{A}^{-1}. \tag{9}$$

Eqs. 5-9 allow us to calculate numerically the differential cross sections of neutrons as a function of k_i and θ, as shown in Fig. 4. Again, for $k_i < k_c$, there are two solutions for each allowed scattering angles. Note that for $k_i < k_c$, the differential cross section diverges at θ_{max}, where the denominator of Eq. 5 vanishes. The integrated cross section, however, remains finite. The total UCN production cross section can now be calculated as a function of k_i using

$$\sigma_{UCN}(k_i) = \int d\sigma/d\Omega\ \theta(E_{UCN} - E_f)\ d\Omega, \tag{10}$$

where the step function θ ensures that the neutrons are produced with an energy E_f below the wall potential E_{UCN}. The results are shown in Fig. 5 for $E_{UCN} = 100, 200, 400$ nev. For a typical UCN wall potential of 200 nev, the useful $\Delta k_i/k_i$ is $\sim 1.2\%$ centered around k_c. The full-width at half-maximum, Δk_{FWHM}, is $\sim 0.006 \mathring{A}^{-1}$.

It is worth noting that the total $n -^4 He$ cross section at $k_c = 0.7038 \mathring{A}^{-1}$ is ~ 0.027 barns [18]. Figure 5 shows that roughly 0.07% of the scattered neutrons end up being UCNs at this incident momentum. This probability drops rapidly as k_i deviates from k_c.

The energy distribution of the produced UCN is also calculated and the result is shown in Fig. 6(a). The energy distribution follows an $E_f^{1/2}$ dependence, in agreement with the prediction of an analytical approach [3].

The angular distributions of the UCNs have also been calculated. Figure 6(b) shows that they are largely isotropic with a small forward-backward asymmetry. For $E_{UCN} =$ 200 nev, the angular distribution is described by $d\sigma/d\Omega \sim 1 + 0.029\ cos\theta$. This result can be compared with an earlier analysis by Lamoreaux and Golub [10].

We are now ready to calculate the expected UCN production rate for the neutron EDM experiment using flight path 12 at LANSCE. The UCN production rate is given by

$$\frac{dN_{UCN}}{dt\ dV} = \int \frac{d\phi}{dk_i}\ \sigma_{UCN}(k_i)\ \rho\ dk_i, \tag{11}$$

where $d\phi/dk_i$ is the flux of incident neutrons, $\sigma_{UCN}(k_i)$ is the UCN production cross section at k_i, ρ is the density of ^4He $(2.18 \times 10^{22} atoms/cm^3)$, and V is the volume of the UCN cell. $d\phi/dk_i$ is practically independent of k_i for the narrow window around k_c. Hence, Eq. 11 becomes

$$\frac{dN_{UCN}}{dt\ dV} = \frac{d\phi}{dk_i}\ \rho \int \sigma_{UCN}(k_i)\ dk_i. \tag{12}$$

For a 200 nev wall potential, $\int \sigma_{UCN}(k_i)\ dk_i = 1.13 \times 10^{-7}$ barns $\mathring{A}^{-1}$. Hence, we obtain

$$\frac{dN_{UCN}}{dt\ dV} = 2.46 \times 10^{-9} \times \frac{d\phi}{dk_i}\ \mathring{A}^{-1}/cm. \tag{13}$$

Based on Fig. V.A.4, the expected flux from flight path 12 for 8.9-$\mathring{A}$ neutrons is $d\phi/dE =$ $5.4 \times 10^7/sec/cm^2/meV$ with 150 μA of protons, which implies $d\phi/dk_i = 1.5 \times 10^8/sec/cm^2/\mathring{A}^{-1}$. Hence,

$$\frac{dN_{UCN}}{dt\ dV} \approx 0.4/sec/cm^3. \tag{14}$$

This value can be compared with our measurement made in December 2002 on flight path 11 that gave $0.56 \pm 0.18/sec/cm^3$ when scaled to flight path 12. The result is also in reasonable agreement with earlier measurements of the production rate [5, 8]. Finally, assuming a UCN storage time of 500 seconds, one obtains a UCN density of ~ 200 per cm^3, a factor of ~ 50 over the recent ILL experiment. The final UCN density will be significantly affected by the transmission of the final stages of the guide, in particular the

losses in polarizing the neutrons. Whereas this part of the experiment is still under development as noted in Appendix A, we use a production rate of $1/sec/cm^3$ for calculations later in the proposal.

If one compares Eq. 13 with Eq. (3.38) of Golub, Richardson, and Lamoreaux [3], the present result is lower than Ref. [3] by roughly 20%. This difference is attributed to the larger value of σ_{coh} used in Ref. [3] ($\sigma_{coh} = 1.3$ barns) than used here ($\sigma_{coh} = 1.1$ barns). We conclude that these two approaches are consistent with each other.

V.B.2 UCN production via the multi – phonon process

It is well known that superfluid ^4He can also have multi-phonon excitations. Unlike the single-phonon excitation which has a delta-function dispersion curve, the multi-phonon process gives a broad energy-versus-momentum band. The location of this multi-phonon band, as measured in a neutron scattering experiment, is shown in Fig. 7. As shown in Fig. 7, the neutron dispersion curve intersects the multi-phonon band at Q around $1.1\mathring{A}^{-1}$. Therefore, UCN could also be produced via the multi-phonon process.

The UCN production cross section via the multi-phonon process can be calculated using the following expression (Eq. (A.11) of Ref. [3] and Eq. 7 of Ref. [14]):

$$\frac{d^2\sigma}{d\Omega\ d\omega} = a_{coh}^2 \frac{k_f}{k_i} S(Q,\omega); \quad S(Q,\omega) = Z(Q)\delta(\omega - \omega(Q)) + S_{II}(Q,\omega). \tag{15}$$

Note that the structure factor contains both the single-phonon part ($Z(Q)$) and the multi-phonon part ($S_{II}(Q,\omega)$). We assume a gaussian distribution for $S_{II}(Q,\omega)$ as follows:

$$S_{II}(Q,\omega) = S_{II}(Q)\frac{1}{\sqrt{2\pi}\sigma(Q)} e^{-(\omega-\omega(Q))^2/2\sigma^2(Q)}. \tag{16}$$

Note that $\int_0^\infty S_{II}(Q,\omega)d\omega = S_{II}(Q)$. $S_{II}(Q)$ is taken from the neutron scattering experiment [14], and the Q-dependence of the centroid ($\omega(Q)$) and width ($\sigma(Q)$) can be extracted from Fig. 7.

We have calculated the multi-phonon UCN production cross sections as a function of k_i, as shown in Fig. 8. Unlike the single-phonon case, the multi-phonon UCN production cross section has a very broad k_i dependence. For a 200 nev wall potential, we obtain $\int \sigma_{UCN}(k_i)dk_i = 0.375 \times 10^{-7} barns \cdot \mathring{A}^{-1}$ for the multi-phonon process. This is aproximately a factor of three lower than the single-phonon cross section. If a broad-band neutron beam is used, the total UCN yield can increase by $\sim 30\%$. However, the increased background created by such a broad-band neutron beam might be too costly for such a modest gain in the UCN yield. Therefore, we believe that a narrow-band neutron beam centered around $8.9\mathring{A}$ would be optimal for UCN production, and the contribution from the multi-phonon process can and should be ignored.

References

[1] R. Golub and J. M. Pendelbury, Phys. Lett. **53A**, 133 (1975).

[2] R. Golub and J. M. Pendelbury, Phys. Lett. **62A**, 337 (1977).

[3] R. Golub, D. J. Richardson, and S. K. Lamoreaux, "Ultra-Cold Neutrons", Adam Hilger, (1991).

[4] P. Ageron, W. Mampe, R. Golub and J. M. Pendelbury, Phys. Lett. **66A**, 469 (1978).

[5] R. Golub et al., Z. Phys. **B51**, 187 (1983).

[6] E. Gustsmiedl, R. Golub and J. Butterworth, Physica **B169**, 503 (1991).

[7] H. Yoshiki et al., Phys. Rev. Lett. **68**, 1323 (1992).

[8] P. R. Huffman et al., Nature **403**, 62 (2000).

[9] C. R. Brome et al., Phys. Rev. **C63**, 055502 (2001).

[10] S. K. Lamoreaux and R. Golub, JETP Lett. **58**, 792 (1995).

[11] R. Golub and S. K. Lamoreaux, Phys. Rev. Lett. **69**, 517 (1992).

[12] G. Placzek and L. Van Hove, Phys. Rev. **93**, 1207 (1954).

[13] M. Cohen and R. P. Feynman, Phys. Rev. **107**, 13 (1957).

[14] R. A. Cowley and A. D. B. Woods, Canadian Journal of Physics, **49**, 177 (1971).

[15] H. J. Maris, Rev. Mod. Phys. **49**, 341 (1977).

[16] A. W. McReynolds, Phys. Rev. **84**, 969 (1951).

[17] R. Golub, Phys. Lett. **72A**, 387 (1979).

[18] H. S. Sommers, J. G. Dash, and L. Goldstein, Phys. Rev. **97**, 855 (1955).

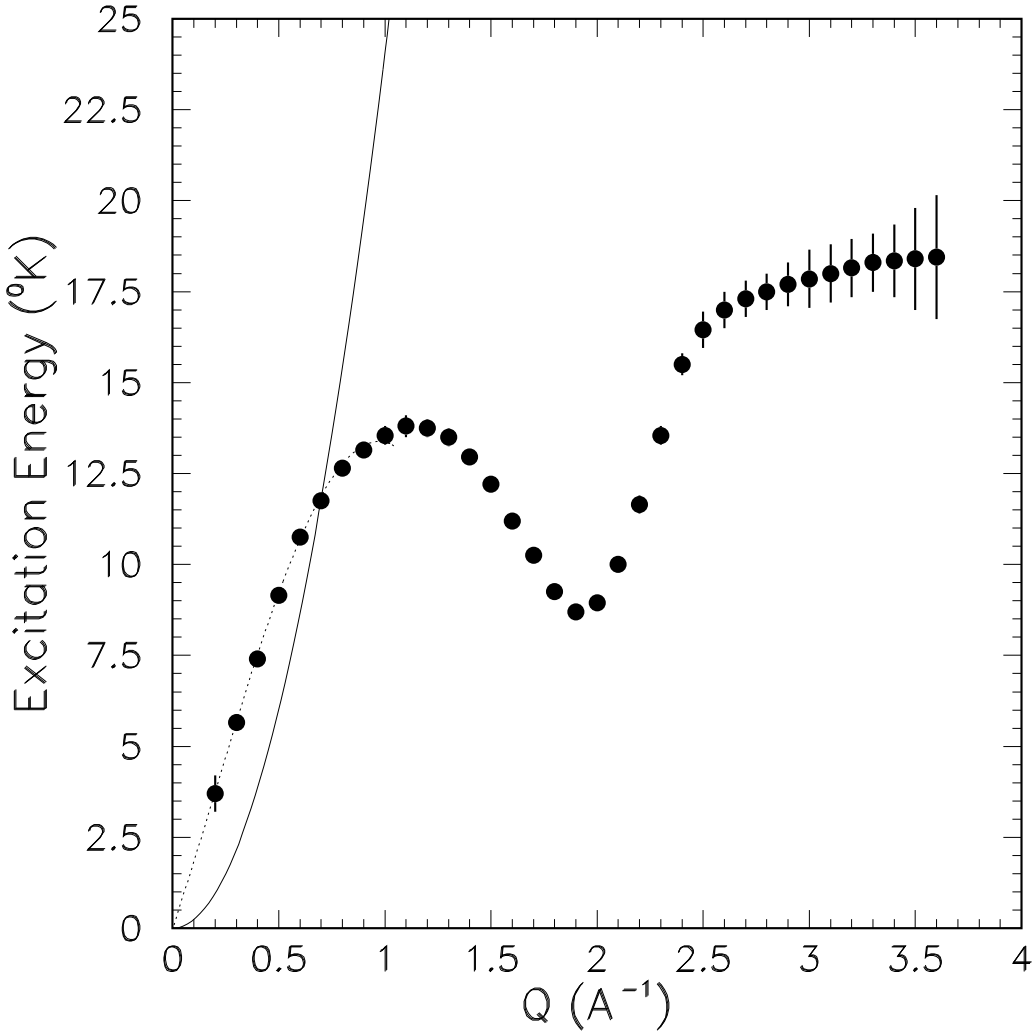

Figure 1: Single-phonon excitation energy (in unit of °K) versus momentum transfer ($\hbar Q$) for superfluid ^4He measured in a cold neutron scattering experiment [14]. The dotted curve is a parameterization by Maris [15]. The solid curve is the energy versus momentum ($E = \hbar^2 Q^2/2M_n$) curve for neutrons.

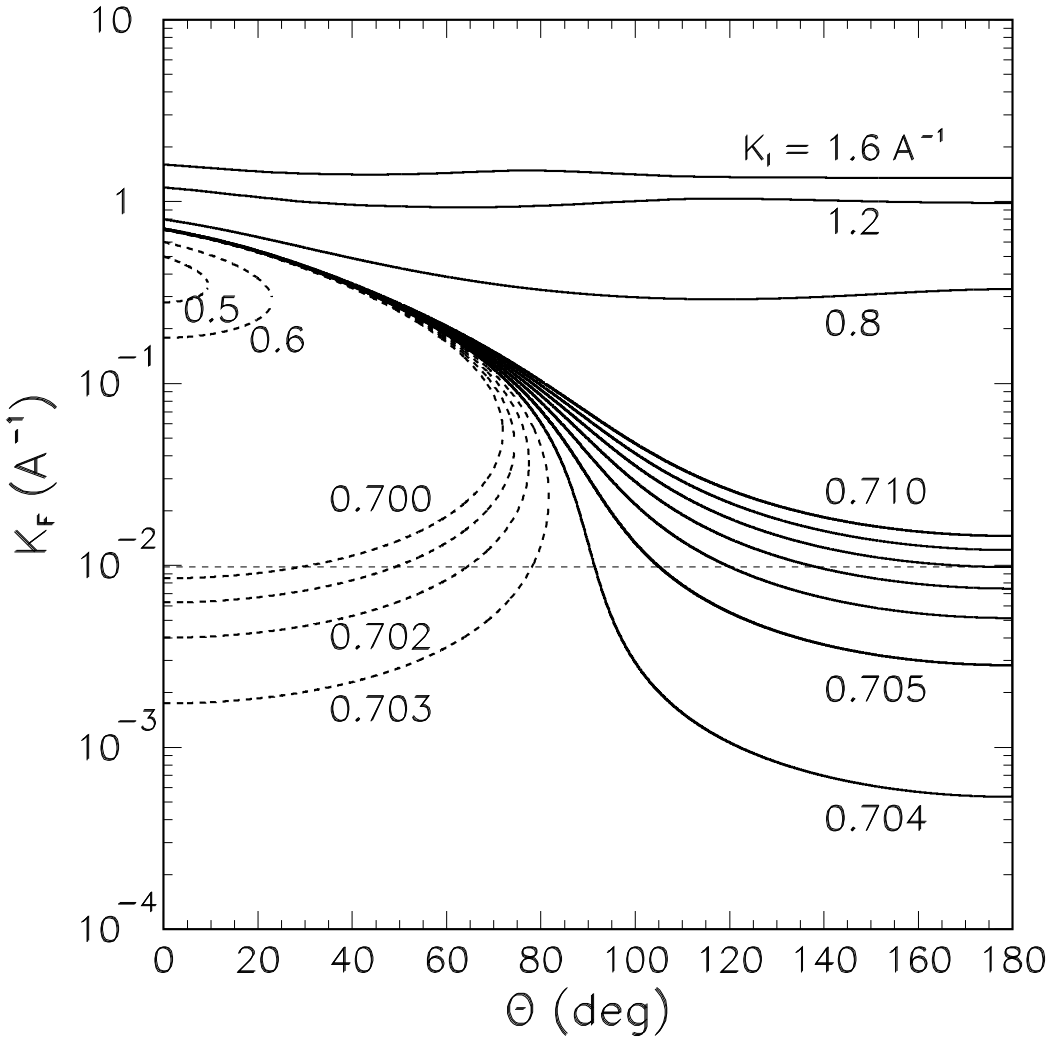

Figure 2: Kinematics of the neutron scattering off a superfluid ^4He target. Momenta of the scattered neutrons (k_F) are plotted as a function of the neutron laboratory scattering angle (θ) for several incident neutron momenta (k_i). The horizontal dashed curve corresponds to a UCN wall potential of 200 nev.

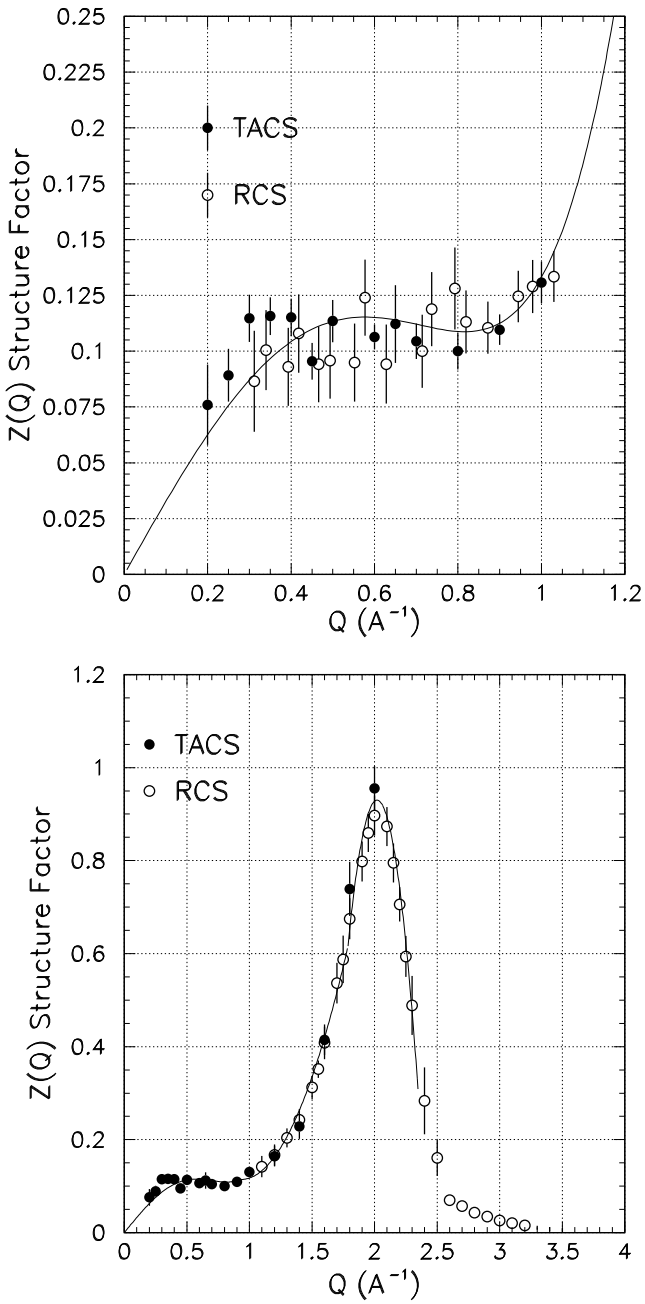

Figure 3: a) Single-phonon structure factor versus momentum transfer for superfluid ^4He measured in a cold neutron scattering experiment [14] using a rotating crystal spectrometer (RCS) and a triple-axis crystal spectrometer (TACS). The solid curve represents a fit [14] to the experimental data. b) Same as a), but for a wider range of momentum transfer. The solid curve represents a fit to the data over the region $Q < 2.35\mathring{A}^{-1}$.

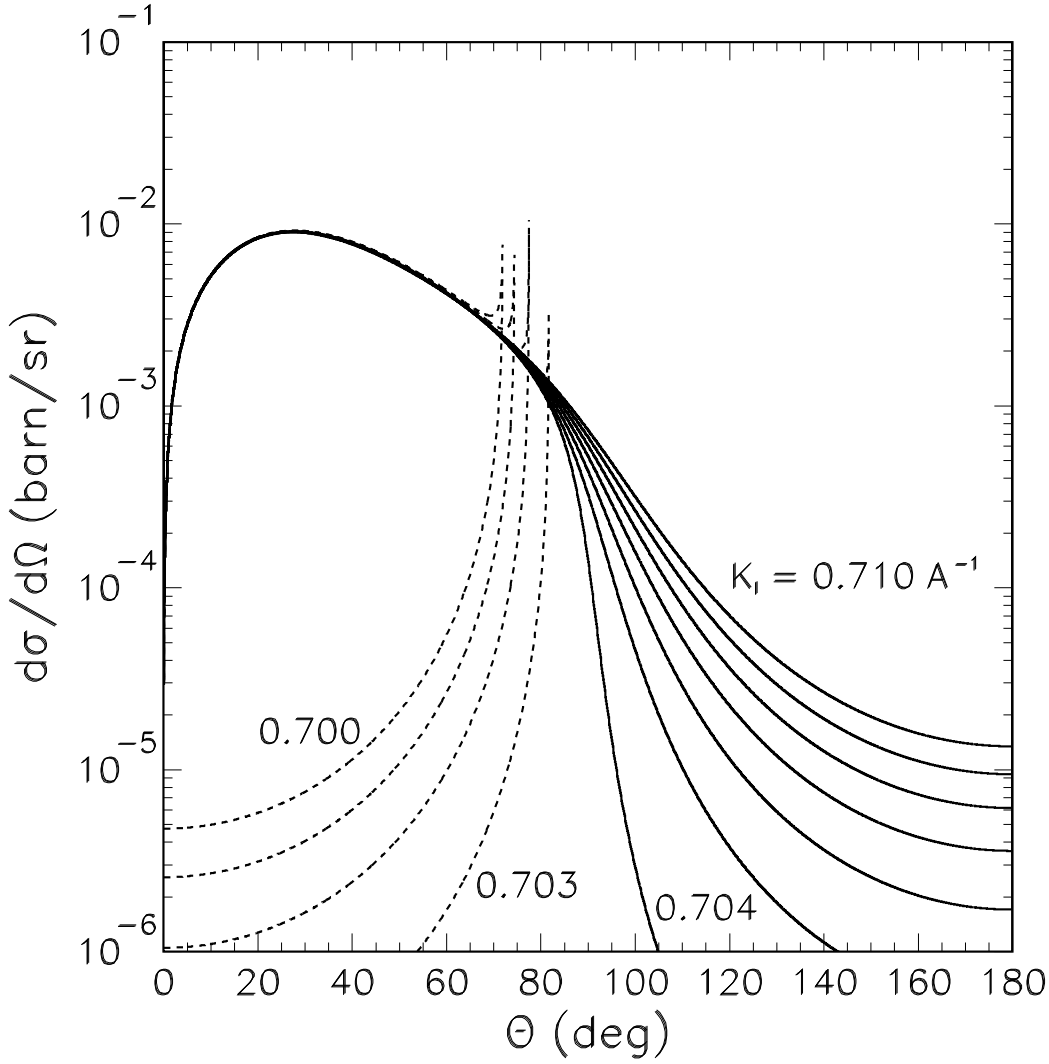

Figure 4: Differential cross sections for neutrons interacting with superfluid ^4He calculated using Eq. 6. For $k_i < k_c$, a singularity of the cross section occurs at θ_{max}.

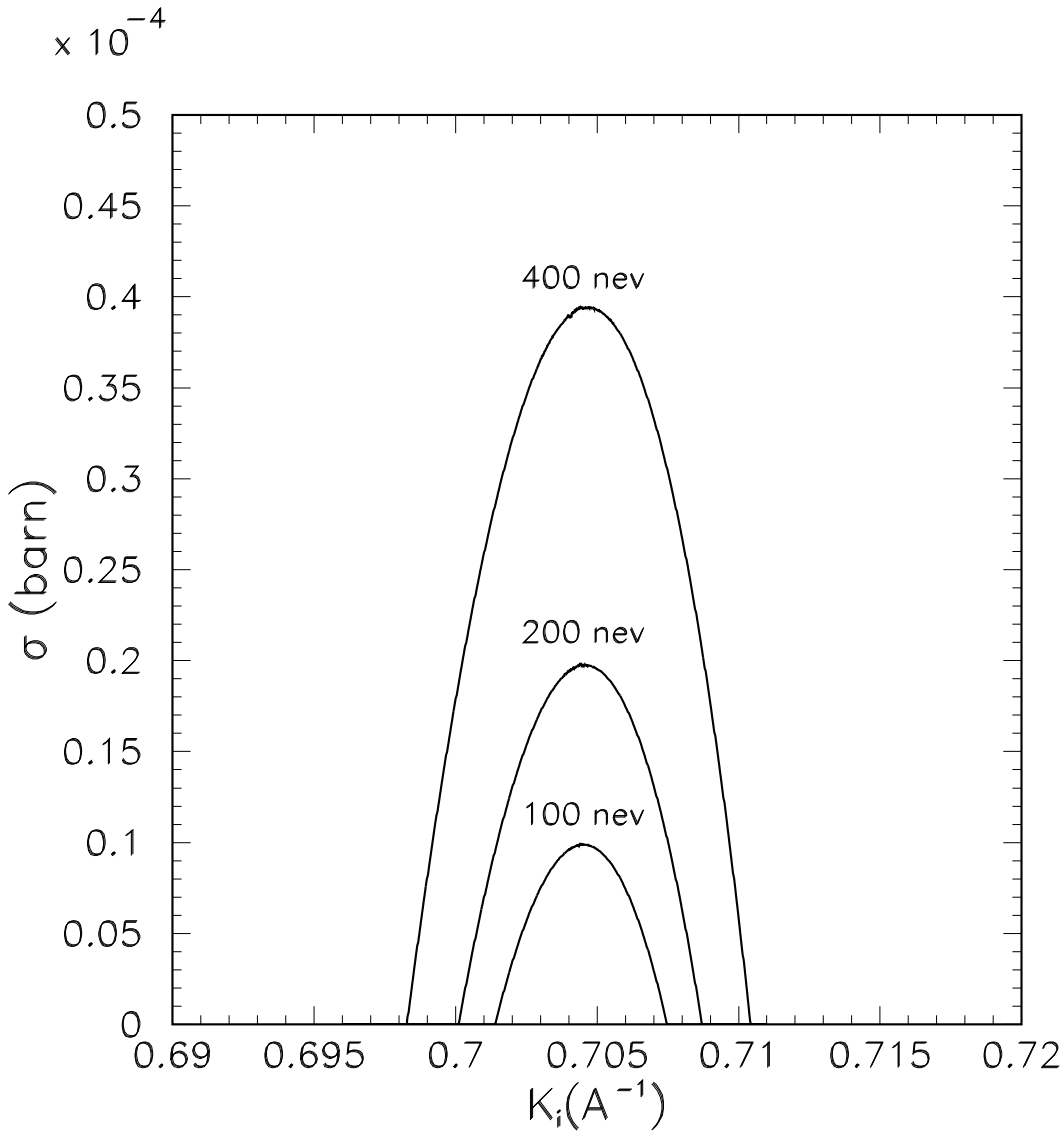

Figure 5: UCN production cross sections in superfluid ^4He via the single-phonon process plotted as a function of the incident neutron wave number, k_i. The three curves correspond to three different wall potentials for containing the UCNs.

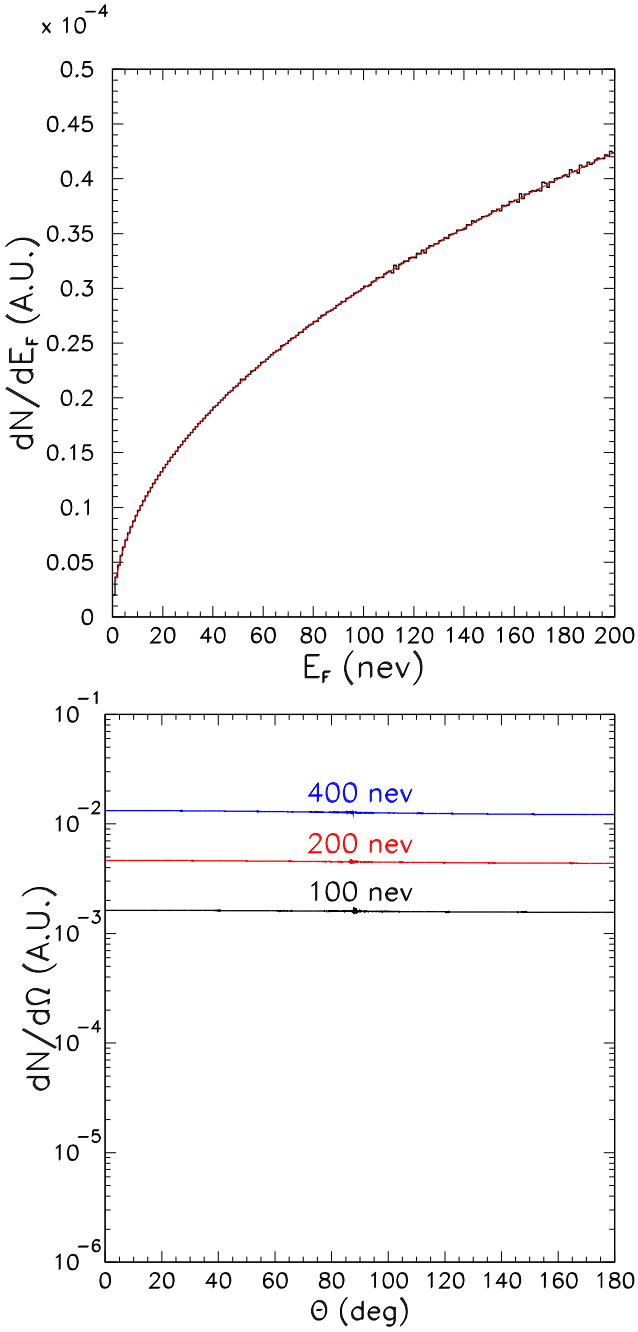

Figure 6: a) Energy distribution of UCN produced in superfluid ^4He calculated using Eq. 6. The solid curve corresponds to a fit, $dN/dE_F \propto E_F^{1/2}$, to the histogram. b) Angular distributions for UCNs produced in superfluid ^4He. Θ is the laboratory angle of UCN with respect to the incident neutron beam direction. The three curves correspond to three different wall potentials for containing the UCNs.

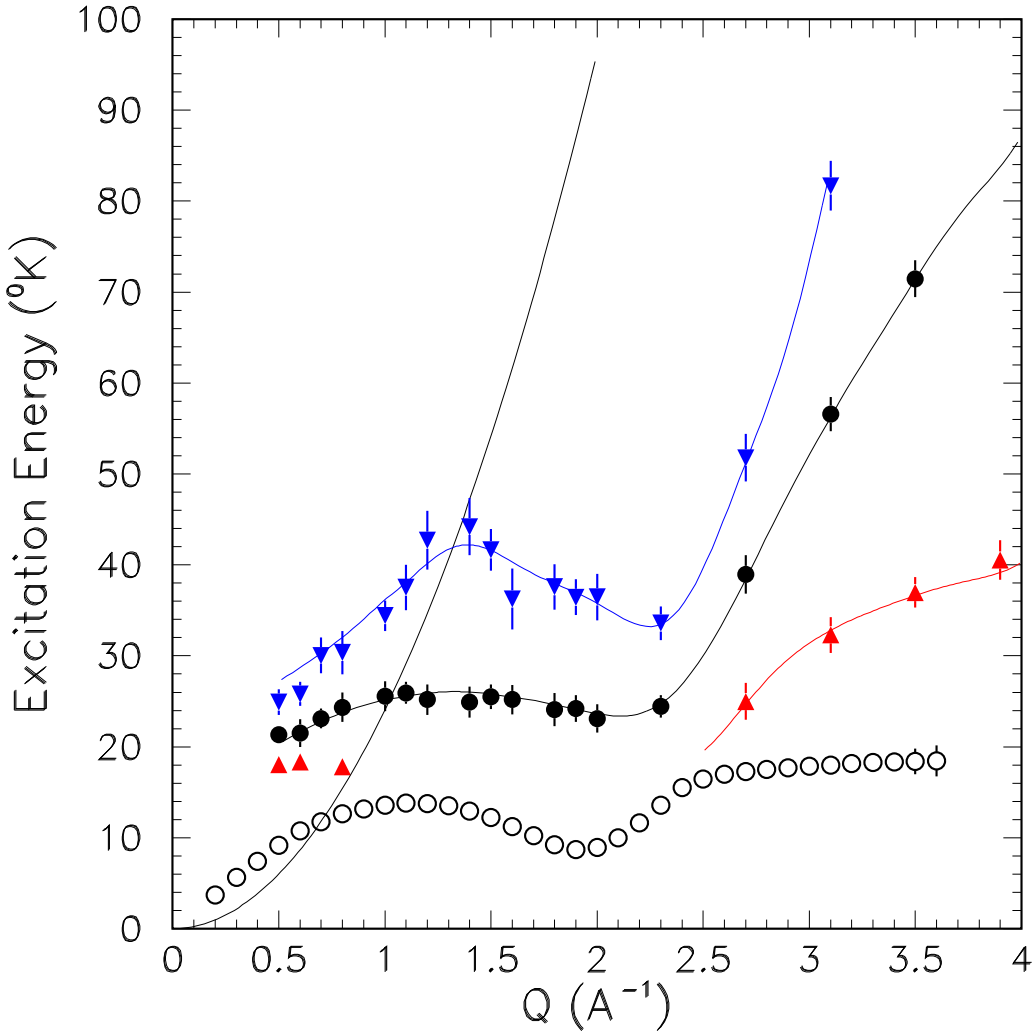

Figure 7: Single-phonon and multi-phonon excitations in superfluid ^4He from Ref. [14]. The open circles indicate the locations of single-phonon excitations. The solid circles correspond to the peak positions for multi-phonon excitations. The triangles mark the locations where the multi-phonon excitation structure factors drop to half of their peak values. The neutron dispersion curve is also shown.

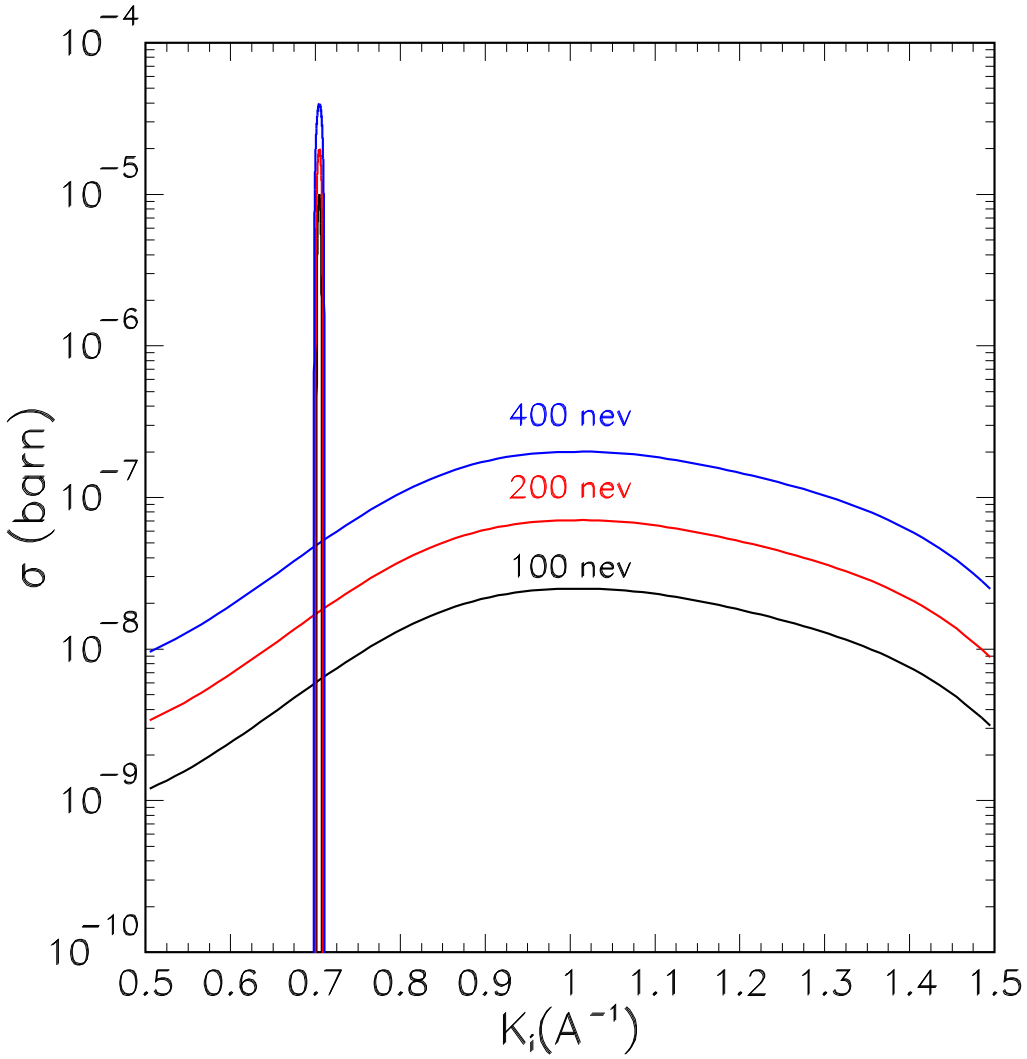

Figure 8: UCN production cross sections in superfluid ^4He via the multi-phonon process plotted as a function of the incident neutron wave number, k_i. The three curves correspond to three different wall potentials for containing the UCNs. The UCN production cross sections via the single-phonon process are also shown as the curves with narrow peaks.